Contents lists available at ScienceDirect

EBioMedicine

Research paper

Imaging epileptic foci in mouse models via a low-density lipoprotein receptor-related protein-1 targeting strategy

Cong Wang[a,b,‡], Jianping Zhang[c,d,e,f,‡], Shaoli Song[e], Zhi Li[g], Shujie Yin[a], Wenjia Duan[a], Zixuan Wei[g], Ming Qi[e], Wanbing Sun[h], Lu Zhang[i], Luo Chen[a], Xihui Gao[j], Ying Mao[g], Hao Wang[b,*], Liang Chen[g,*], Cong Li[a,*]

[a] Key Laboratory of Smart Drug Delivery, Ministry of Education, School of Pharmacy, Fudan University, Shanghai, China
[b] National Pharmaceutical Engineering Research Center, China State Institute of Pharmaceutical Industry, Shanghai, China
[c] Institute of Modern Physics, Fudan University, Shanghai, China
[d] Shanghai Engineering Research Center for Molecular Imaging Probes, Shanghai, China
[e] Department of Nuclear Medicine, Shanghai Cancer Center, Fudan University, Shanghai, China
[f] Key Laboratory of Medical Molecular Virology (MOE/NHC/CAMS), School of Basic Medical Sciences, Fudan University, Shanghai, China
[g] Department of Neurosurgery, Huashan Hospital, Fudan University, Shanghai, China
[h] Department of Neurology, Shanghai Changhai Hospital, Second Military Medical University, Shanghai, China
[i] Department of Neurology, Huashan Hospital, Fudan University, Shanghai, China
[j] School of Basic Medical Sciences, Fudan University, Shanghai, China

ARTICLE INFO

ABSTRACT

Background: In the setting of drug-resistant epilepsy (DRE), the success of surgery depends on the ability to accurately locate the epileptic foci to be resected or disconnected. However, the epileptic foci in a considerable percentage of the DRE patients cannot be adequately localised. This warrants the need for a reliable imaging strategy to identify the "concealed" epileptic regions.
Methods: Brain specimens from DRE patients and kainate-induced epileptic mouse models were immunostained to evaluate the integrity of the blood-brain barrier (BBB). The expression of low-density lipoprotein receptor-related protein-1 (LRP1) in the epileptic region of DRE patients and kainate models was studied by immunofluorescence. A micellar-based LRP1-targeted paramagnetic probe (Gd^{3+}-LP) was developed and its ability to define the epileptic foci was investigated by magnetic resonance imaging (MRI).
Findings: The integrity of the BBB in the epileptic region of DRE patients and kainate mouse models were demonstrated. LRP1 expression levels in the epileptic foci of DRE patients and kainate models were 1.70−2.38 and 2.32−3.97 folds higher than in the control brain tissues, respectively. In vivo MRI demonstrated that Gd^{3+}-LP offered 1.68 times higher ($P < 0.05$) T1-weighted intensity enhancement in the ipsilateral hippocampus of chronic kainite models than the control probe without LRP1 specificity.
Interpretation: The expression of LRP1 is up-regulated in vascular endothelium, activated glia in both DRE patients and kainate models. LRP1-targeted imaging strategy may provide an alternative strategy to define the "concealed" epileptic foci by overcoming the intact BBB.
Funding: This work was supported by the National Natural Science Foundation, Shanghai Science and Technology Committee, Shanghai Municipal Science and Technology, Shanghai Municipal Health and Family Planning Commission and the National Postdoctoral Program for Innovative Talents.

1. Introduction

As a brain disorder characterized by an enduring predisposition to generate seizures, epilepsy affects ~65 million people worldwide [1]. Despite the availability of a wide range of antiepileptic drugs, approximately 30% of epilepsy patients still experience uncontrollable seizures, which leads to neuropsychiatric and neuropsychological comorbidities, social disability, a decline in quality of life and an increase in mortality [2]. For patients with drug-resistant epilepsy

* Corresponding author.
E-mail addresses: wanghao10@sinopharm.com (H. Wang), chenlianghs@126.com (L. Chen), congli7511@gmail.com (C. Li).
‡ These authors contributed equally to this work.

Research in context

Evidence before this study

Surgery is the mainstay treatment for the DRE patients. The identification of the epileptic foci is a prerequisite for applying surgical intervention. MRI is essential for the presurgical assessment of epileptic foci due to its excellent spatial resolution for soft tissues. However, approximately 30% of DRE patients have no distinct structural abnormality in MRI. These patients benefit less from surgery even in combination with other invasive and non-invasive diagnostic strategies. Therefore, it is of clinical significance to identify the reasons leading to the failure of lesion delineation and construct an imaging strategy to define the "concealed" epileptic foci.

Added value of this study

Intact BBB structure with the evidence of unspoiled inter-endothelial tight junction was presented in the resected epileptic tissues of DRE patients. The expression of LRP1, a neuroinflammation-related receptor, increased significantly in epileptic tissues from both refractory epilepsy patients and epileptic mouse models. The fabricated LRP1-targeted MR contrast agent helps to locate the epileptic foci by overcoming the BBB in epileptic mouse models.

Implications of all the available evidence

Patients with refractory epilepsy without a detectable brain lesion have limited therapeutic options. The results from our study showed the commercially available imaging probe may fail in locating epileptic foci when the BBB is relatively intact. The LRP1-targeted contrast agent provides a promising strategy that can be used in complement with current methodologies used to locate epileptic foci with high spatial resolution.

(DRE), surgery is an effective way to alleviate seizures and even achieve a seizure-free status by excising the epileptic foci defined as the minimum amount of cortex that must be resected or disconnected [2,3]. Surgical prognosis strongly depends on the presurgical localisation of the epileptic foci [4]. The odds of being seizure-free after surgery is 2−3 times greater if aberrant lesions such as hippocampal sclerosis could be identified in structural magnetic resonance imaging (MRI) [5]. However, the epileptic lesions in approximately 30% of DRE patients cannot be accurately identified. These patients usually are subjected to additional imaging studies, including single-photon emission computed tomography (SPECT), 18-fluoro-deoxy-glucose positron emission tomography (^{18}F-FDG PET) or magnetoencephalography [6]. Nevertheless, the epileptic foci in a considerable percentage of DRE patients still cannot be adequately localised even in combination with an intracranial electroencephalogram [7]. Accordingly, reliable surrogate approaches visualising the "concealed" epileptic foci are urgently needed.

Blood-brain barrier (BBB) dysfunction and the associated leakage of serum proteins have been recognised as a pathological hallmark of the epileptic brain. Contrast-enhanced MRI has been used to noninvasively locate the epilepsy foci by tracking the paramagnetic contrast agent leaked from the disrupted BBB [8]. However, a considerable number of DRE patients do not show any distinct aberrances in structural MR images after the administration of the contrast agents such as Gd^{3+}-DTPA [9−11]. Nevertheless, the histological analysis reveals that the epileptic lesions exist in 87% of these patients after surgery [12]. We envisage that the epileptic lesions with intact BBB result in the failure of current imaging strategies to

locate them. Therefore, imaging probes with BBB permeability are needed for comprehensively delineating the "concealed" epileptic foci.

A rapidly growing body of clinical and preclinical evidence demonstrates that chronic neuroinflammation is accompanied by epilepsy [13]. Activated astrocytes and microglia are prominent phenomena of epileptic tissues in DRE patients [14]. Disruption of glial-mediated regulation of neurotransmitters, ions, water and immunity facilitates epileptogenesis by increasing neuronal excitability [14]. Low-density lipoprotein receptor-related protein-1 (LRP1) is a transmembrane receptor actively involved in cargo transport, cell signalling and endocytosis [15]. LRP1-targeted imaging probes and drug delivery vectors showed enhanced BBB permeability via the LRP1 mediated transcytosis [16,17]. Increased LRP1 expression is found in the tissues where the neuroinflammation occurs [18]. For example, LRP1 up-regulation in the microglia, astrocytes, endothelial cells, pericytes and oligodendrocytes in response to inflammatory stimuli was reported in brain disorders such as multiple sclerosis [19]. With the sustainable neuroinflammation during epileptogenesis, we speculate that LRP1 expression level will increase in epileptic foci. The up-regulated LRP1 in the activated endothelial and glial cells will facilitate the BBB traverse of the imaging probes and be a reliable biomarker to define the epileptic foci.

In this work, we assume that the LRP1 can be a reliable neuroinflammation associated biomarker for defining the epileptic foci. To verify the above hypothesis, the integrity of BBB and the expression of LRP1 in the epileptic tissues of DRE patients were investigated. An LRP1-targeted paramagnetic probe (Gd^{3+}-LP) was developed and its ability to locate the epileptic foci in chronic seizure models was investigated by *in vivo* MRI. Overall, this work demonstrates that LRP1 could be a potential biomarker for imaging the "concealed" epileptic foci with relatively intact BBB.

2. Methods

2.1. Materials

Solvents and chemicals, if not specified, were purchased from Tokyo Chemical Industry (Tokyo, Japan) or Sigma Aldrich (St. Louis, MO) and used without further purification. Cysteine-angiopep2 peptide (TFFYGGSRGKRNNFKTEEYC, MW = 2404.6) was purchased from China Peptides Co (Jiangsu, China). Methoxypoly(ethylene glycol) 2000-poly(lactic acid)2000 (PEG-PLA) and maleimide-PEG-PLA (Mal-PEG-PLA) were provided by Shanghai Ponsure Biotech (Shanghai, China). Gadolinium (Gd-DTPA, Magnevist) was purchased from Bayer HealthCare Pharmaceuticals, Inc (Clayton, NC).

2.2. Ethics

The project was approved by the institutional review board (ethical committee) of Huashan Hospital (ethics approval number KY2015-256), and the written informed consent was obtained from all patients. The protocol for animal experiments was carried out in accordance with institutional animal welfare guidelines and approved by the ethics committee of Fudan University.

2.3. Specimens

Human specimens were acquired from DRE patients who underwent a craniotomy at the Department of Neurosurgery, Huashan Hospital in 2019. Epileptic tissues were excised from five DRE patients (2 males, age: 22−30 years; 3 females, age: 21−30 years, detailed information is available in Table S1). The control brain samples were collected from normal-appearing hippocampi of three autopsy specimens from patients without a history of seizures.

2.4. Synthesis and characterisation

PEG-PLA-diethylenetriaminepentaacetic acid (DTPA) was synthesised according to the previous work with minor modification [20]. Briefly, a mixture of PEG-PLA (200 mg, 50 μmol), and DTPA dianhydride (72 mg, 0.2 mmol) in 5.0 mL anhydrous N,N-Dimethylformamide was stirred thoroughly with triethylamine (20 mg, 0.2 mmol) for 48 h at room temperature. The final product PEG-PLA-DTPA was purified by dialysing against deionised water followed lyophilisation. Coupling of Mal-PEG-PLA (41 mg, 10 μmol) and cysteine-angiopep2 peptide (24 mg, 10 μmol) was carried out in a mixture of N,N-Dimethylformamide/phosphate buffer saline (PBS, pH 7.4) (1:1, V/V) at room temperature. After stirring at room temperature overnight, the product was purified by dialysing against deionised water followed lyophilisation. PEG-PLA-[Gd^{3+}-DTPA] was synthesised by adding $GdCl_3 \bullet 6H_2O$ (36.7 mg, 0.06 mmol) and PEG-PLA-DTPA (400 mg, 0.1 mmol) into a mixture of 4-(2-hydroxyethyl)-1-piperazineethanesulfonic acid buffer (pH 6.5) and dioxane (1:1, V/V) at 50 °C. The product was purified by dialysing against deionised water followed lyophilisation. For probe preparation, a mixture of PEG-PLA (10.0 mg, 2.5 μmol), PEG-PLA-[Gd^{3+}-DTPA] (9.0 mg, 2.0 μmol), and angiopep2-PEG-PLA (1.0 mg, 0.16 μmol) was dissolved in dimethyl sulfoxide (1.0 mL) and then dialysed against ultrapure water. The resulted suspension was filtrated with polyethersulfone syringe filter (0.45 μm, Merck Millipore, Milford, MA), and then concentrated with centrifugal filtration units (Amicon Ultra, 10 kDa, Millipore, Milford, MA). Freshly prepared probe Gd^{3+}-LP was used immediately in the following imaging experiments. Gd^{3+}-labelled control probe (Gd^{3+}-CP) was developed with a similar procedure as Gd^{3+}-LP but by the replacement of angiopep2-PEG-PLA with PEG-PLA.

The contents of Gd^{3+} in samples were determined by inductively coupled plasma-atomic emission spectrometry (Hitachi P-4010, Hitachi, Tokyo, Japan) with radio-frequency power at 1100 W and nebulise gas flow at 0.9 L/min. The morphology and size of Gd^{3+}-LP were examined under a high-resolution transmission electron microscope (JEM-2010, JEOL Ltd., Tokyo, Japan). The hydrodynamic diameter and zeta potential were determined in a disposable zeta potential cell using Malvern Zetasizer ZS90 (Zetasizer Nano ZS90, Malvern Instruments Ltd., Worcestershire, UK) at 25 °C. The study flowchart was shown in Fig. S1.

2.5. Radiochemical synthesis and characterisation

PEG-PLA-[^{99m}Tc-DTPA] was synthesised with stannous chloride as described below. PEG-PLA-DTPA (5 mg, 1.2 μmol) and stannous chloride (20 μL, 5.0 mg/mL, pH 2.0) were dissolved in 0.5 mL phosphate buffer saline (pH 5.5–6.5). Freshly eluted technetium 99 m pertechnetate (185 MBq in 300 μL saline) was added. After reaction for 30 min at 40 °C, the mixture was purified by Sep-Pak C-18 Cartridge (Waters, Milford, MA). The radiochemical purity of PEG-PLA-[^{99m}Tc-DTPA] was determined by high-performance liquid chromatography on a HITACHI system (D-7100, Merck-Hitachi, Tokyo, Japan) equipped an analytical C18 column (250 mm × 4.6 mm, pore size: 5.0 μm) and a gamma counter. The flow rate was 1.0 mL/min by using isocratic mobile phase with 10% A (0.1% trifluoroacetic acid in acetonitrile) and 90% B (0.1% trifluoroacetic acid in water) during the first 0–6 min, then a gradient mobile phase going from 10% A at 6 minute to 90% A at 7 min, and further by isocratic mobile phase with 90% during 7–20 min. The purified PEG-PLA-[^{99m}Tc-DTPA] (20 μL, 37 MBq) was incubated at 37 °C in phosphate buffer saline (180 μL) or mouse serum (180 μL) for 24 h. The stability of the complex was determined by measuring the radiochemical purity (n = 3) at selected time points (0,1,4,12, and 24 h) by paper chromatography. Before testing, the mixture was treated with 0.2 mL of acetonitrile and then centrifuged at 14,000 rpm for 2 min to precipitate the serum protein. Paper chromatography was performed on Xinhua no.1 filter paper

with normal saline as the mobile phase. ^{99m}Tc-LP was prepared with a similar procedure as Gd^{3+}-LP but the replacement of PEG-PLA-[^{99m}Tc-DTPA] with PEG-PLA-[Gd^{3+}-DTPA].

2.6. In vitro MRI study

A volume of 200 μL Gd^{3+}-LP or Gd^{3+}-DTPA solution with different gadolinium concentrations was added into microplates. The microplates were fixed on the pad, and in vitro MR phantom study was performed under a 7.0 T small animal MR scanner (PharmaScan; Bruker, Billerica, Mass). T1-weighted MR images were acquired using the Spin echo sequence (500/6.17 ms of repetition time/echo time, 5 averages). For the T1 mapping study, the field of view was set to 75 ▯ 60 mm, slice thickness = 1.5 mm, echo time = 6.02 ms and repetition time = 44, 300, 800, 1500, 3000 ms, 2 averages.

2.7. Establishment of kainate models

The C57BL/6 mice (4–6 weeks old, male; Slac Lab Animal Ltd., Shanghai, China) were anaesthetised with 1–2% isoflurane and kainate (0.3 μg) was injected into basal hippocampal at the following coordinates from bregma (anteroposterior = -2.0 mm, mediolateral = -1.8 mm, dorsoventral = -2.0 mm) and maintained in place for 5 min to avoid reflux. Seizure behaviors were recorded for at least 2 h post kainite administration and the animal models were classified according to a modified Racine scale [21] (Table S2). Mice reached grade 4–6 and lasted for at least 1 h were selected for the subsequent studies. Sham surgery mice were injected with saline. Mice were monitored by two independent observers who were blinded to the treatment for at least 2 h daily. After a latent phase, the chronic kainate mice with spontaneously recurrent seizures were selected for the subsequent imaging studies. See Fig. S2 for a schematic overview of the SE induction and the development of chronic epilepsy models. Mice were housed in adjoining individual cages, maintained with light (standard 12/12 h light/dark cycle), controlled temperature and humidity (23 °C and 50% humidity), and given access to standard pellet feed and water ad libitum. At the end of the follow-up, mice were euthanized by isoflurane overdose inhalation, followed by cervical dislocation to ensure death.

2.8. Electroencephalogram studies

The kainate mice and saline-treated control mice were anaesthetised with 1–2% isoflurane and then implanted with a handmade stainless steel screw electrode in the epidural space at the following location: the recording electrode (anteroposterior = -2.0 mm, mediolateral = -1.8 mm) and the reference electrode was placed over the cerebellum. The electrodes were fixed on the skull with dental acrylic cement. The electrophysiological signals were acquired using a NeuroLog System (Digitimer Ltd., Hearts, UK) at a sampling rate of 50 kHz, bandpass filtered from 0.5 to 6 kHz, amplified 1000 times. A notch filter of 50 Hz was used to remove power line interference. The epileptiform activity was defined according to the previously published guidelines [22,23].

2.9. Immunofluorescence staining studies

The mouse or human brain tissues were fixed in 4% formaldehyde solution, dehydrated and sectioned with a thickness of 10 μm. The slices were permeabilised with 0.3% Triton X-100 and then blocked with immune staining blocking buffer (P0102, Beyotime, Shanghai, China) for 1 h and incubated with corresponding primary antibody overnight at 4 °C. The following antibodies were used: mouse platelet/endothelial cell adhesion molecule-1 (CD31) monoclonal antibody (1:200 dilution, ab24590, Abcam, Cambridgeshire, UK, RRID: AB_448167), rabbit zonula occludens-1 (ZO-1) polyclonal antibody

(1:50 dilution, 61-7300, Thermo Fisher, Slangerup, Denmark, RRID: AB_2533938), rabbit LRP1 monoclonal antibody (1:200 dilution, ab92544, Abcam, Cambridgeshire, UK, RRID: AB_448167), rat glial fibrillary acidic protein (GFAP) monoclonal antibody (1:200 dilution, 13-0300, Thermo Fishers, Slangerup, Denmark, RRID: AB_2532994), and goat ionised calcium-binding adaptor molecule 1 (Iba1) poly-clonal antibody (1:50 dilution, NB100-1028, Novus Biologicals, Little-ton, Colorado, RRID: AB_521594). After washing thoroughly, the slices were incubated with Alexa Fluor 647-labelled goat anti-rabbit secondary antibody (1:200 dilution, 33113ES60, YEASEN, Shanghai, China), Cy3-labelled goat anti-rat secondary antibody (1:200 dilution, 33308ES60, YEASEN, Shanghai, China) or Alexa-fluo488-labelled goat anti-mouse secondary antibody (1:200 dilution, 33206ES60, YEASEN, Shanghai, China) at room temperature for 1 h followed by nucleus staining with 4',6-diamidino-2-phenylindole (DAPI, 0.5 mg/mL) for 5 min. The immunofluorescence images were collected on ZEISS LSM 700 Confocal Laser Scanning Microscope (Carl Zeiss, Dresden, Germany). The fluorescence intensities of the images were quantified by Image J (version 1.46, NIH, Bethesda, MA).

2.10. Immunohistochemistry

The human brain tissues were fixed and dehydrated as described in the immunofluorescence studies mentioned in the manuscript. Then the tissues were embedded in paraffin and sectioned with a thickness of 5 μm. Tissue slices were deparaffinised, rehydrated in descending series of ethanol and microwaved in citrate buffer (10 mM, pH 6.0) for 8 min. Endogenous peroxidases were blocked with 3% hydrogen peroxide and washed with phosphate buffer (pH 7.2, 10 mM). The slices were blocked in 2% fetal bovine serum in 0.1 M Tris buffer, and then incubated with the following primary antibody overnight at 4 °C: rabbit LRP1 monoclonal antibody (1:1000 dilution, ab92544, Abcam, Cambridgeshire, UK, RRID: AB_2234877), GFAP monoclonal antibody (1:500 dilution, 13-0300, Thermo Fisher, Waltham, Mass, RRID:AB_2532994), and Iba1 polyclonal antibody (1:500 dilution, NB100-1028, Novus Biologicals, Littleton, Colorado, RRID: AB_521594). After incubation with horseradish peroxidase enzyme-labelled secondary antibody, slices were developed using the diaminobenzidine detection kit (DET-HP1000, MilliporeSigma, St Louis, MO, USA) according to the manufacturer's instructions. Slices were then counterstained with hematoxylin. Immunoreactivity was evaluated under an optical microscope (Olympus BX51, Olympus, Tokyo, Japan) with the aid of a BIOPAD digital camera (DP72; Olympus, Tokyo, Japan).

2.11. Immunoblotting

The ipsilateral hippocampus of the mice was excised, washed with cold PBS (0.01 M, pH7.4) and then lysed by RIPA buffer with 1% protease inhibitor cocktail. The samples were homogenised and centrifuged (14,000 rpm) for 20 min. The protein concentrations of the supernatants were determined by BCA assay. Protein (15 μg) from each sample was separated by 10% SDS PAGE at 80 V for 20 min and 160 V for 40 min, and then transformed to polyvinylidene difluoride membrane at 90 V for 90 min in an ice bath. After blocked with 5% nonfat milk in TBS-T (50 mM Tris-HCl, 150 mM NaCl, 0.1% Tween-80), the membrane was incubated with mixed primary antibody overnight at 4 °C. The following antibodies were used: rabbit LRP1 monoclonal antibody (1:20000, Abcam, ab92544, Cambridgeshire, UK, RRID: AB_2234877), rabbit GAPDH polyclonal antibody (1:10000, Abcam, ab70699, Cambridgeshire, UK, RRID: AB_1209569). After washing thoroughly, the membranes were incubated with HRP-conjugated goat anti-rabbit secondary antibody (1:10000, YEASEN) for 1 h at room temperature. Super electrochemiluminescence (ECL) detection Reagent (Yeasen Biotech Co, S1827521) was used to

visualise the immunoblots and Quantity One software (Bio-Rad) was used to quantify the immune-activities.

2.12. In vivo SPECT/CT studies

Small animal SPECT/CT imaging was performed on a Nano SPECT/CT (Bioscan Inc., Washington, DC) with a 4-head multiplexing multi-pinhole camera. ^{99m}Tc-LP or control tracer ^{99m}Tc-CP (5.6−7.4 MBq) was injected intravenously into kainate models in the acute, latent and chronic phases respectively. CT image was acquired over 180 projections by using a 0.15 mA 45 kVp x-ray tube on a flat-panel detector (exposure time: 500 ms). SPECT was acquired under the following parameters: four high-resolution conical collimators with 9-pinhole plates; energy peak, 140 keV; full width, 20%; resolution, 1 mm/pixel; matrix, 256 × 256; and scan time, 30 s/projection, 24 projections in all. All acquired SPECT data were reconstructed with HiSPECT (version 1.4.2870; Scivis GmbH, Göttingen, Germany). SPECT and CT data were automatically coregistered and analysed using dedicated fusion software (invivoscope, version 1.44; Bioscan, Inc., Washington, DC).

2.13. Bio-distribution studies

Kainate models (n = 4 per group) were intravenously injected with ^{99m}Tc-LP (2.45−2.61 MBq) and sacrificed at 0.5 h after injection. Tissues of interest (blood, heart, liver, lungs, kidneys, spleen, brain, intestine, stomach, and thyroid) were excised and weighed. The radioactivity of each organ was measured by a gamma counter (SN-684, Shanghai Hesuo Rihuan Photoelectric Instrument Co., Ltd., Shanghai, China). The decay-corrected activity per mass of tissue was calculated and the activity level was expressed as the percentage of the injected radioactive dose per gram of tissue (% ID/g).

2.14. In vivo MRI studies

Kainate models in chronic phase (n = 12) and sham models (n = 4) were used for in vivo MRI with a 7.0 T small animal MR scanner (PharmaScan; Bruker Biospin, Billerica, MA). The animal models were anaesthetised and maintained with 1−2% isoflurane in 20% oxygen. In vivo coronal MR images of mouse brain were acquired using a transmit/receive quadrature volume radiofrequency coil with an inner diameter of 38 mm before and at selected time points after i.v. injection of contrast agents Gd^{3+}-LP and Gd^{3+}-CP (0.1 mmol Gd/Kg). Coronal T2-weighted MRI was acquired with turbo-rapid acquisition with relaxation enhancement sequences sequences: time of repetition/time of echo = 2500/33 ms, acquisition matrix = 256 × 256; number of excitation = 4, field of view = 20 × 20 mm; number of slices = 9; slice thickness = 0.8 mm, rare factor = 8. The rapid acquisition with relaxation enhancement sequences was used for T1-weighted MRI: time of repetition/time of echo = 1500/6 ms; acquisition matrix = 256 × 256, number of excitations = 2; field of view = 20 × 20 mm; number of slices = 9, slice thickness = 0.8 mm, rare factor = 4.

2.15. In vivo PET/CT studies

Helical CT and PET scans of mice were obtained with an Inveon micro-PET/CT (Preclinical Solutions; Siemens Healthcare Molecular Imaging, Knoxville, TN). The mice fasted for more than 6 h before image acquisition. Each mouse received 7.4 ± 0.3 MBq ^{18}F-FDG via the lateral tail vein. Isoflurane (2%) in oxygen was used to anesthetize the mouse during the scanning period. The images were acquired under the following parameters: 120 projections per bed position, 360° of rotation, 500 μA anode source transmitting 80 keV X-ray with an exposure time of 300 ms, X-ray detector of 3072 transaxial pixels × 2048 axial pixels.

2.16. Nissl staining studies

Mouse brains were harvested, fixed and dehydrated as described in the immunofluorescence studies mentioned above. Then the tissues were embedded in paraffin and sectioned with a thickness of 5 μm. The slices were deparaffinised and then stained with 1% cresyl violet solution. The stained slices were observed under the optical microscope (Olympus BX51, Olympus, Tokyo, Japan). The number of surviving intact hippocampal CA1 and CA3 pyramidal cells per 1 mm length was counted in every fifth section under a light microscope.

2.17. Statistical analysis

The sample sizes were determined according to previous experimental experience. We excluded data from animals that died before experimental termination. Model mice were randomly applied to all experiments. Blinding was applied to the in vivo SPECT/CT, MRI and PET/CT experiments. Quantitative data obtained were all expressed as mean $\pm$ standard deviation unless stated otherwise. Statistical differences between two groups were tested with a two-tailed Student's t-test. For all the tests, 95% confidence interval of difference (95% CI of diff.) was used to estimate the difference between the two groups. Values of $P < 0.05$ were regarded as a statistically significant difference, n.s $P > 0.05$, *$P < 0.05$, **$P < 0.01$, ***$P < 0.001$, ****$P < 0.0001$. All statistical calculations were performed using Prism (version 7.00.; GraphPad Software).

2.18. Role of the funding source

The funders of the manuscript had no role in the study design, data collection, data analysis, data interpretation, or writing of the manuscript.

3. Results

3.1. Intact BBB structures existed in the epileptic regions of DRE patients

Three patients received Gd^{3+}-DTPA for gadolinium-enhanced MRI. However, none of the patients showed T1-weighted MR signal enhancement in epileptic foci, which indicated that the BBB structure remained partially intact in the lesions (Fig. S3). To further investigate the BBB integrity in epileptic foci, ZO-1 protein was immuno-stained in the resected epileptic tissues from DRE patients. As shown in Fig. 1a, ZO-1 immunity was presented as continuous and sharp strips along the lumen side of brain vascular endothelium in the control brain tissues. Notably, the inter-endothelial tight junction structures kept intact in large parts of the lesions, even though the disrupted ZO-1 immunity was indeed observed in the lesions (Fig. 1a). In comparison to the control human brain tissues, no significant down-regulation of ZO-1 expression level (95% CI of diff [-0.067, 0.25]; $P = 0.24$; two-tailed Student's t-test) was observed in the epileptic tissues (Fig. 1b).

3.2. Up-regulated LRP1 demonstrated in the epileptic regions of DRE patients

LRP1 expression level on the vascular endothelium in the epileptic lesion from DRE patients was 1.70 ± 0.3 folds higher than that in the control human brain tissues (95% CI of diff [-0.80, -0.21]; $P = 0.0037$; two-tailed Student's t-test) (Figs. 2a and b). The activation of astrocytes and microglia were evident with morphological changes manifested as cell body enlargement and branches thickening (Fig. 2c and e). Compared to the control human brain tissue, the LRP1 expression level was increased by 2.38 ± 0.3 folds on astrocytes (95% CI of diff [-0.61, -0.25]; $P = 0.0011$; two-tailed Student's t-test) and 2.18 ± 0.3 folds on microglia (95% CI of diff [-0.53, -0.20]; $P = 0.018$; two-tailed
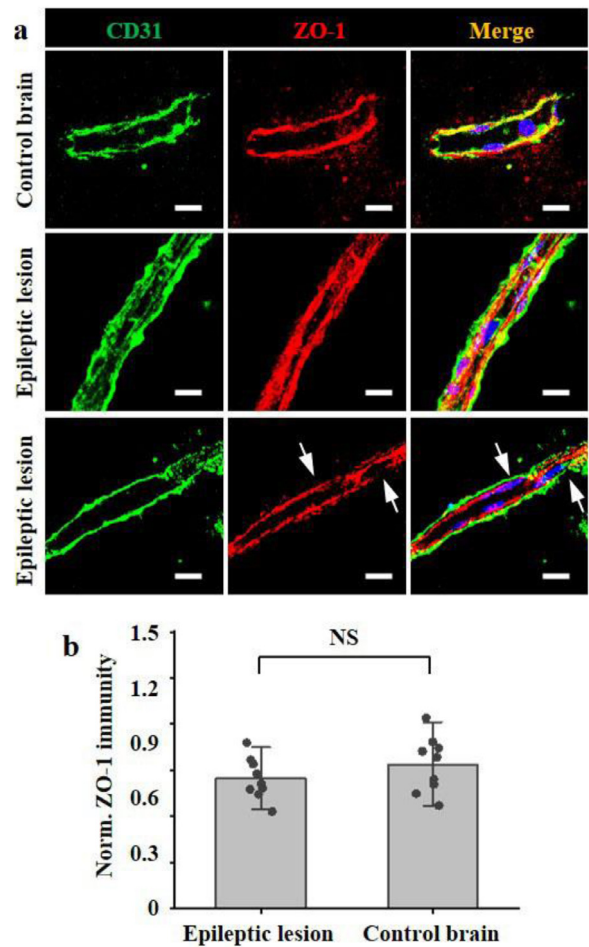
Fig. 1. Intact BBB structures existed in the epileptic foci of DRE patients. (a) Representative immunofluorescence images of vascular endothelium and para-endothelial tight junctions in the epileptic and control brain tissues. Endothelium stained by CD31 antibody was displayed in green, tight junction-associated protein ZO-1 immunity was displayed in red; the nucleus stained with DAPI was shown in blue. The locations with disrupted ZO-1 immunity were indicated with white arrows. Scale bar = 10 μm. (b) Normalized vascular ZO-1 immunities in epileptic and control brain tissues (n = 9). Norm. = normalized. n.s $P > 0.05$, unpaired two-tailed Student's t-tests.

Student's t-test) (Fig. 2d and f). Similar reactive gliosis and LRP1 up-regulation were also found in the epileptic lesion by immunohistochemistry (Fig. S4).

3.3. Synthesis and characterisation of Gd^{3+}-LP

A micellar-based magnetic resonance contrast agent Gd^{3+}-LP was prepared through the self-assembly of PEG-PLA-[Gd^{3+}-DTPA] with other synthesised functional polymer monomers via the dialysis method (Fig. 3a). As shown in figure Fig. 3b, Gd^{3+}-LP showed a well-organised spherical structure with a diameter of 10−15 nm. The hydrodynamic size was approximately 26 nm due to the swelling of micelle in aqueous solution and zeta potential was + 8.2 mV as detected by dynamic light scattering (Fig. 3c). As Fig. S5 displays, Gd^{3+}-LP showed desirable stability and maintained good monodispersity after storing at room temperature for three days. Also, histological HE staining showed no apparent damage to the main organs of the mice even at a high dosage (0.5 mmol [Gd^{3+}]/kg) (Fig. S6). T1-weighted images of phantom showed an increased signal intensity with increased concentrations of Gd^{3+}-LP (Fig. 3d). T1-weighted MR images of phantom showed the calculated r_1 relaxivity for Gd^{3+}-LP was 11.8 mM^{-1}s^{-1}, which was remarkably higher than that of clinically available contrast agent Gd^{3+}-DTPA (3.9 mM^{-1}s^{-1}) (Fig. 3e).
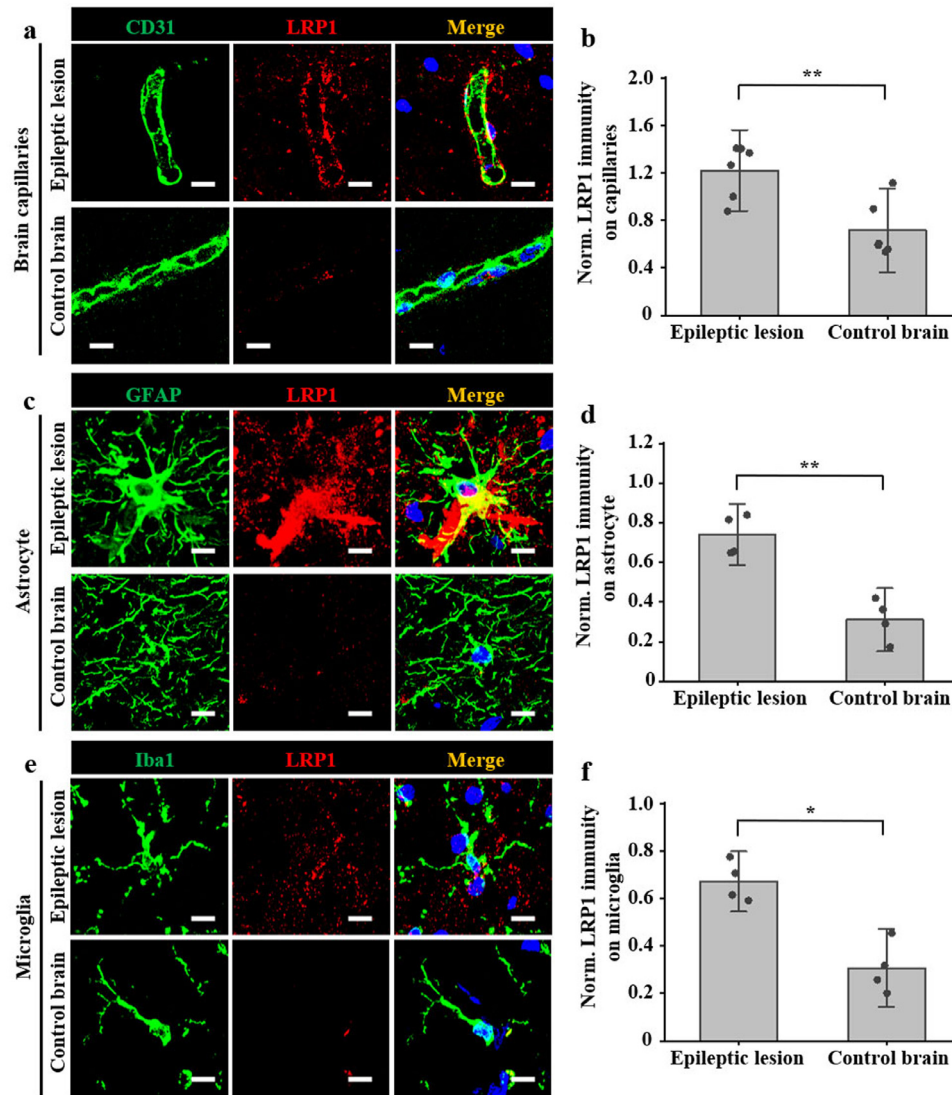
Fig. 2. LRP1 upregulation was demonstrated in multiple cell types in the epileptic foci of DRE patients. Representative LRP1 immunofluorescence images of vascular endothelium (a), astrocytes (c), microglia (e) in the epileptic tissues and control brain tissues. Scale bar = 10 μm. Endothelium stained by CD31 antibody, astrocyte stained by GFAP, and microglia stained by Iba1 were displayed in green, LRP1 immunity was displayed in red; the nucleus stained with DAPI were shown in blue. Normalized LRP1 immuno-intensities in vascular endothelium (n = 6) (b), astrocytes (n = 4) (d), microglia (n = 4) (f) in the epileptic tissues and control brain tissues. Norm.: normalized. $^*P < 0.05$, $^{**}P < 0.01$, unpaired two-tailed Student's t-tests.

Radioactive tracer ^{99m}Tc-LP was prepared with the identical strategy to Gd^{3+}-LP except the replacement of PEG-PLA-[Gd^{3+}-DTPA] with PEG-PLA-[^{99m}Tc-DTPA]. ^{99m}Tc-LP showed similar hydrodynamic size and zeta potential to Gd^{3+}-LP (Fig. S7 and S8).

3.4. LRP1 up-regulation in kainate models

The epileptic mouse model was prepared by *in situ* injection of kainate into the hippocampus. Representative subdural electroencephalogram and energy spectra of the epileptic models during epileptogenesis were shown in Fig. S9. While clear paroxysmal discharges were observed in the acute phase, occasionally isolated low voltage spikes were observed in the latent phase. Notably, the spontaneous paroxysmal discharge was evident in the chronic phase. In contrast, only background electroencephalogram signal with typical desynchronised activity was observed in saline-treated control mice. The LRP1 immunofluorescence intensity increased obviously in the acute phase compared with the saline-treated group (3.93 ± 1.0 folds in CA1, 95% CI of diff [-3.0, -1.2]; $P < 0.0001$; two-tailed Student's t-test) (3.97 ± 1.4 folds in CA3, 95% CI of diff [-3.4, -1.2];

$P < 0.0001$; two-tailed Student's t-test) (3.75 ± 0.3 folds in the dentate gyrus, 95% CI of diff [-3.1, -1.5]; $P < 0.0001$; two-tailed Student's t-test) (Fig. 4a−c). In comparison to the acute phase, the LRP1 level decreased in the latent phase (0.62 ± 0.1 folds in CA1, 95% CI of diff [0.15, 2.0]; $P = 0.019$; two-tailed Student's t-test) (0.60 ± 0.2 fold in CA3, 95% CI of diff [0.13, 2.4]; $P = 0.026$; two-tailed Student's t-test) (0.62 ± 0.1 folds in dentate gyrus, 95% CI of diff [0.38, 2.0]; $P = 0.0028$; two-tailed Student's t-test) but basically unchanged in the chronic phase (95% CI of diff [-0.68, 1.1] in CA1; $P = 0.90$; two-tailed Student's t-test) (95% CI of diff [-1.1, 1.2] in CA3; $P = 1.00$; two-tailed Student's t-test) (95% CI of diff [-0.86, 0.74] in dentate gyrus; $P = 1.00$; two-tailed Student's t-test) (Fig. 4c). It is worth noting that there are good colocalisations between the immunities of LRP1 and CD31, Iba1, GFAP, indicating the up-regulated LRP1 on the vascular endothelium, activated microglia and astrocytes (Fig. S10). Moreover, the activation of astrocytes increased constantly, and severely reactive astrogliosis and glial scar formation were observed in the chronic phase (Fig. 4a). The increased microgliosis was seen in the acute phase post-SE with bushy and amoeboid morphologies in the hippocampus (Fig. 4b). However, the activated microglia partially returned
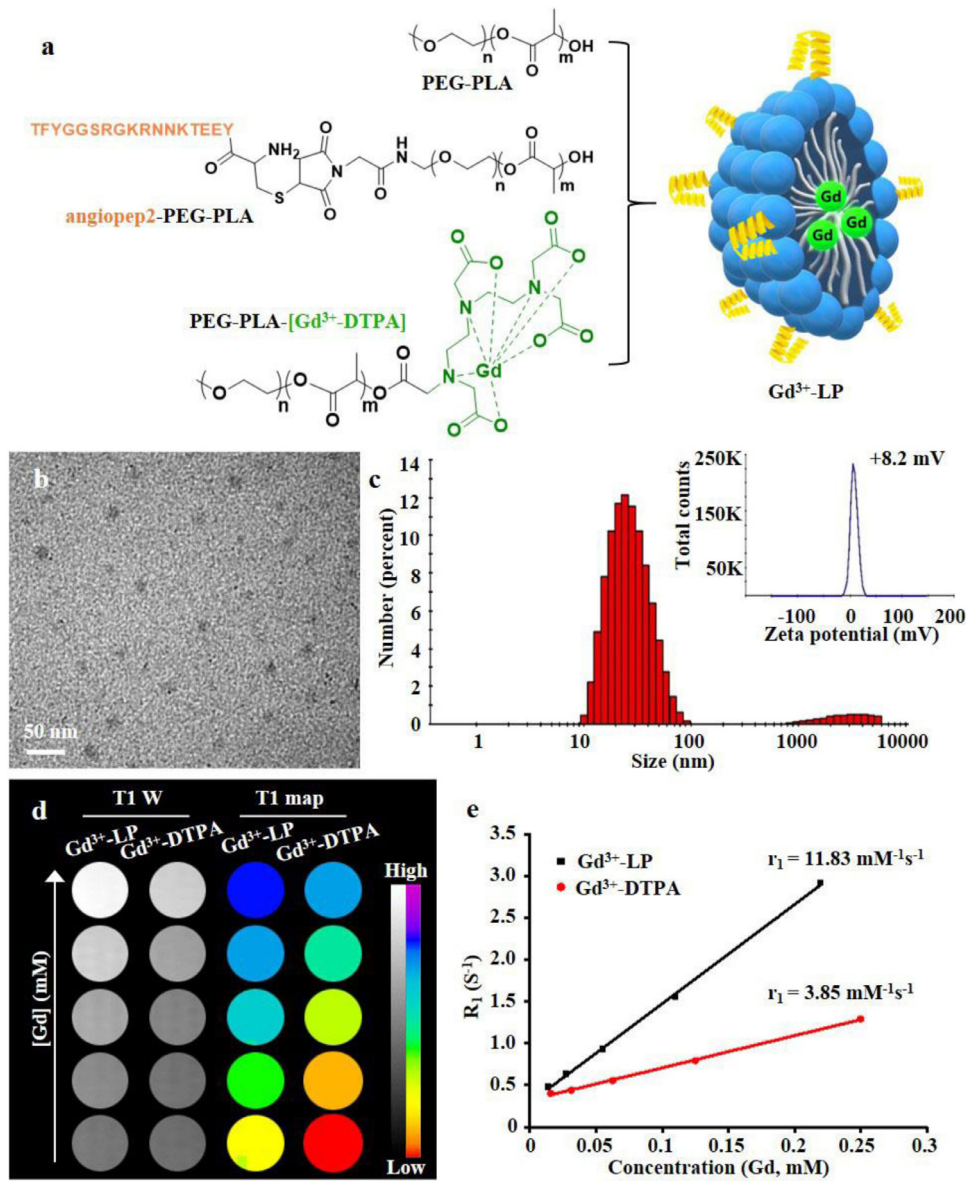
Fig. 3. Synthesis and characterisation of Gd^{3+}-LP. (a) Gd^{3+}-LP was developed via self-assembly of polymer monomers including PEG-PLA, angiopep2-PEG-PLA and PEG-PLA-[Gd^{3+}-DTPA]. (b) The transmission electron microscope image of Gd^{3+}-LP. Scale bar = 50 nm. (c) Hydrodynamic size distribution patterns and zeta potential of Gd^{3+}-LP. (d) *In vitro* MR phantom images of Gd^{3+}-LP and Gd^{3+}-DTPA as a function of Gd^{3+} concentrations. (e) Plotting longitudinal relaxation time (R_1) with Gd^{3+} concentration offers the relaxivity (r_1) of Gd^{3+}-LP and Gd^{3+}-DTPA.

to their surveying phenotype during the latent phase (Fig. 4b and e). Similarly, western blots also showed that LRP1 expression was increased in the acute (95% CI of diff [0.13, 0.39]; *P* = 0.0025; two-tailed Student's *t*-test) and chronic phase (95% CI of diff [0.11, 0.43]; *P* = 0.0056; two-tailed Student's *t*-test), while marginally changed in the latent phase (95% CI of diff [-0.0034, 0.23]; *P* = 0.055; two-tailed Student's *t*-test) (Fig. S11).

3.5. Imaging LRP1 expression during epileptogenesis with SPECT in kainate models

The expression of LRP1 was further assessed *in vivo* with SPECT/CT after intravenous administration of ^{99m}Tc-LP. We observed the increased uptake of the ^{99m}Tc-LP in the ipsilateral hippocampus in kainate models but not in the contralateral hemisphere (Fig. 5a). Quantitative results showed that the ^{99m}Tc-LP uptake ratio between ipsilateral hemisphere and contralateral hemisphere was higher than that of ^{99m}Tc-CP without LRP1 targeting specificity (5.67 ± 1.1 vs 2.70 ± 0.8, acute phase, 95% CI of diff [-5.1, -0.82]; *P* = 0.019; two-

tailed Student's *t*-test) (4.35 ± 0.7 vs 2.42 ± 0.6, latent phase, 95% CI of diff [-3.5, -0.37]; *P* = 0.026; two-tailed Student's *t*-test) (4.55 ± 1.0 vs 1.83 ± 0.7, 95% CI of diff [-4.7, -0.75], chronic phase; *P* = 0.019; two-tailed Student's *t*-test) (Fig. 5b). Consistent with the SPECT/CT data, biodistribution study also indicated the increased uptake of ^{99m}Tc-LP in the ipsilateral hippocampus in comparison to the contralateral hippocampus in the acute phase (3.68 ID/g ± 0.8 vs 2.28 ID/g ± 0.6, 95% CI of diff [-2.4, -0.17]; *P* = 0.030; two-tailed Student's *t*-test) and chronic phase (3.06 ID/g ± 0.3 vs 2.03 ID/g ± 0.5, 95% CI of diff [-1.7, -0.32]; *P* = 0.012; two-tailed Student's *t*-test) (Fig. 5c). Predominant liver uptake (> 25%ID/g) and intestine uptake (> 10%ID/g) of ^{99m}Tc-LP was observed (Fig. 5c).

3.6. Gd^{3+}-LP visualising the epileptic foci in chronic epilepsy mouse models

In vivo MRI was conducted to investigate if the LRP1-targeted strategy could be used to image the epileptic foci. The chronic seizure mouse models were randomly divided into three groups and
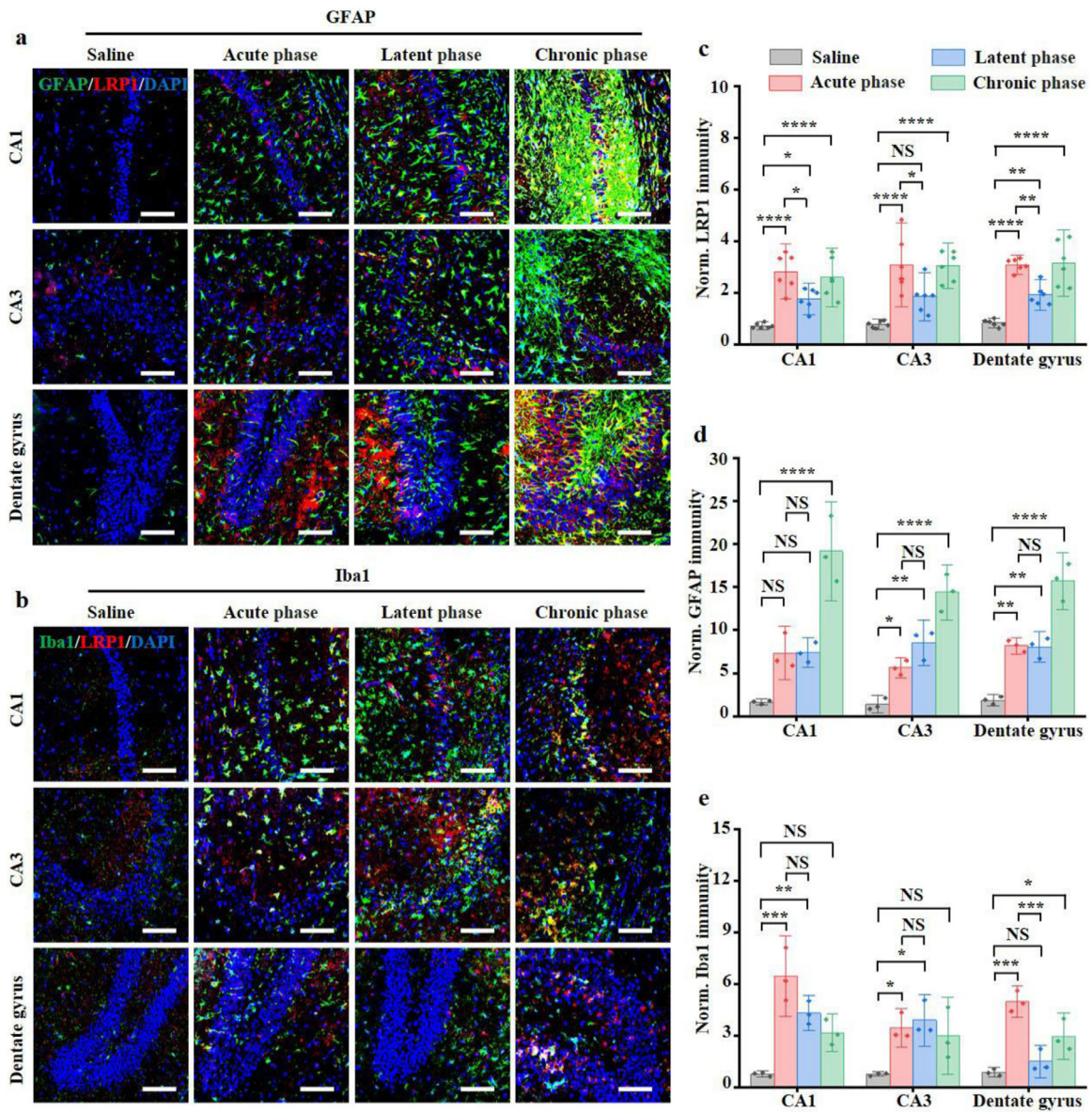
Fig. 4. LRP1 up-regulation during epileptogenesis in kainate models. (a, b) Representative immunofluorescence images of hippocampus from saline-treated mice and kainate models. Astrocyte stained by GFAP and microglia stained by Iba1 were displayed in green. LRP1 immunity was displayed in red. The nucleus stained with DAPI were shown in blue. Scale bar = 100 μm. Normalized vascular LRP1 immunities (n = 6) (c), GFAP immunities (n = 3) (d), Iba1 immunities (n = 3) (e) in saline-treated mice and kainate models. Norm. = normalized. n.s $P > 0.05$, $^*P < 0.05$, $^{**}P < 0.01$, $^{***}P < 0.001$, $^{****}P < 0.0001$, unpaired two-tailed Student's t-tests.

intravenously injected with Gd^{3+}-LP, Gd^{3+}-CP or Gd^{3+}-DTPA with the same gadolinium concentration (0.1 mmol/kg). In the fourth group, the sham mice were injected with Gd^{3+}-LP. As shown in Fig 6a, obvious T1-weighted MR signal enhancement was observed in the ipsilateral hippocampus of kainate models at 90 min post-injection of Gd^{3+}-LP. In contrast, less MR signal enhancement was observed after injecting Gd^{3+}-CP without LRP1 specificity (95% CI of diff [-0.081, -0.012]; $P = 0.017$; two-tailed Student's t-test) or sham models with Gd^{3+}-LP (95% CI of diff [-0.13, -0.060]; $P = 0.0006$; two-tailed Student's t-test) (Fig. 6b). It is worth noting that minor MR signal enhancement was observed after injecting Gd^{3+}-DTPA, which verifies the BBB was relatively intact in the chronic seizure mouse. Interictal ^{18}F-FDG PET is another important investigation for presurgically localising epileptogenic brain regions with the characteristics of cerebral hypometabolism [24]. As shown in Fig. S12, brain regions with enhanced MR signal after Gd^{3+}-LP administration spatially colocalised with the hypo-metabolic region indicated by interictal ^{18}F-FDG PET. Nissl staining showed that irreversible damages of hippocampal

pyramidal neurons characterized as loss of cell morphology and pyknosis of nucleus in the hippocampus region indicated with the hyper-intensive signal in T1-weighted MR images (Fig. 6c).

4. Discussion

Accurately defining the epileptic foci is essential in improving prognosis of the DRE patients. However, the epileptic foci of a considerable percentage of the patients cannot be adequately localised even combining all the current diagnostic strategies. These patients suffer from uncontrolled seizures, low quality of life and higher mortality due to limited therapeutic options. Therefore, a more sensitive and accurate imaging approach for epileptic foci location is clinically needed.

In the present study, we first tried to elucidate why the existing imaging technology could not adequately define the epileptic lesions in a considerable percentage of DRE patients. BBB plays a vital role in maintaining brain homeostasis and is an obstacle for intracerebral
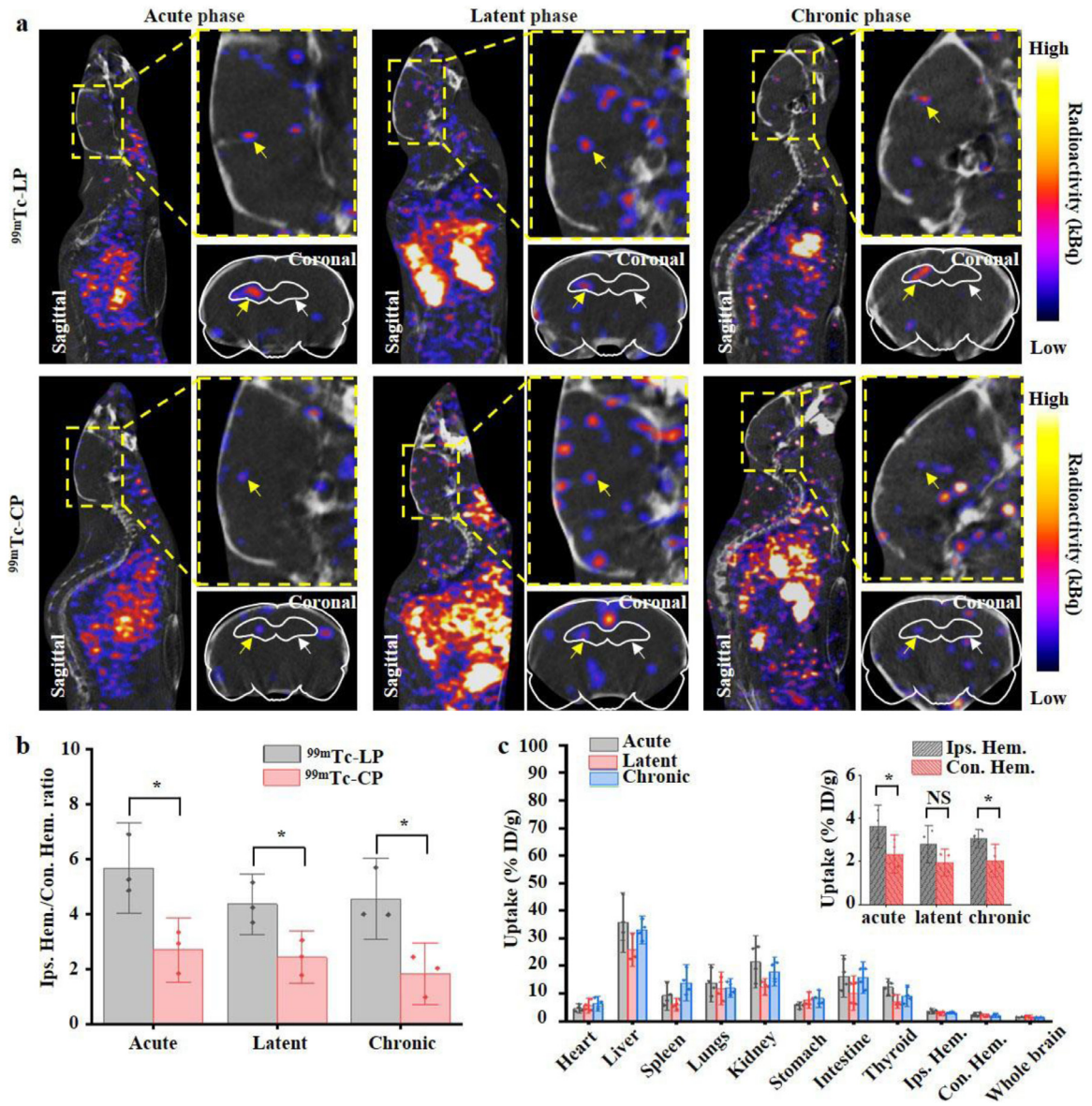
Fig. 5. Persistent LRP1 upregulations during epileptogenesis in kainate models. (a) SPECT/CT images of kainate models at 0.5 h post intravenous administration of ^{99m}Tc-LP or control tracer ^{99m}Tc-CP in the acute, latent and chronic phase. In the coronal section, yellow and white arrows point to the ipsilateral hippocampus and contralateral hippocampus, respectively. Additionally, the hippocampus and brain were outlined with white lines. (b) The bar chart shows the mean ipsilateral hemisphere to contralateral hemisphere radioactivity per unit volume ratio (n = 3). (c) Bio-distribution of ^{99m}Tc-LP in kainate models at 0.5 h post intravenous administration (n = 4). Ips. Hem. = ipsilateral hemisphere, Con. Hem. = contralateral hemisphere. n.s $P > 0.05$, $^*P < 0.05$. unpaired two-tailed Student's t-tests.

delivery of imaging agents [25]. Inter-endothelial tight junctions are key structures maintaining BBB integrity and preventing the blood-derived substances from entering the brain parenchyma [26]. Considering the intact BBB structures with unspoiled tight junction structure in the resected epileptic tissues of DRE patients, an imaging strategy overcoming BBB is required to comprehensively delineate the epileptic foci.

Receptor-mediated endocytosis is a promising way to efficiently transport large molecules from blood stream into the brain [27]. Multiple receptors expressed on the luminal side of brain vascular endothelium have been exploited, such as lactoferrin receptor, transferrin receptor, insulin receptor, and LRP1 [27]. In this study, we demonstrated that the LRP1 expression was up-regulated on brain capillary endothelial cells, activated astrocytes and microglia in the epileptic regions of DRE patients. Accordingly, angiopep-2, a 19-amino acid peptide derived from aprotinin (a peptide ligand for LRP1 LRP1 ligand), was selected as an LRP1 targeted ligand due to its superior transcytosis capacity to that of aprotinin and transferrin [28].

Paramagnetic T1-weighted contrast agents are usually preferred in the clinic by providing the hyper-intensive signal that is easily identified in the MR images. Covalent binding of paramagnetic contrast agents to a macromolecule is an effective way to increase the T1 relaxivity by extending rotational correlation time τ_R of the paramagnetic chelators [29]. The T1 relaxivity of Gd^{3+}-LP was determined as three times higher than Gd^{3+}-DTPA. Additionally, the multiple angiopep−2 peptides modified on the Gd^{3+}-LP increase its BBB permeability via multivalent effect between Gd^{3+}-LP and LRP1 receptors [30].

As the most frequently used drug-resistant epilepsy models for preclinical studies, the kainate-induced rodent models have demonstrated the advantages including developmental convenience, good reproducibility and high similarity to human temporal lobe epilepsy in the aspect of behavioural manifestation, neuropathological changes and electrophysiologic features [31]. Convulsive status epilepticus with unilateral or bilateral forelimb clonus, rearing and falling were observed 20−120 min post kainate injection.
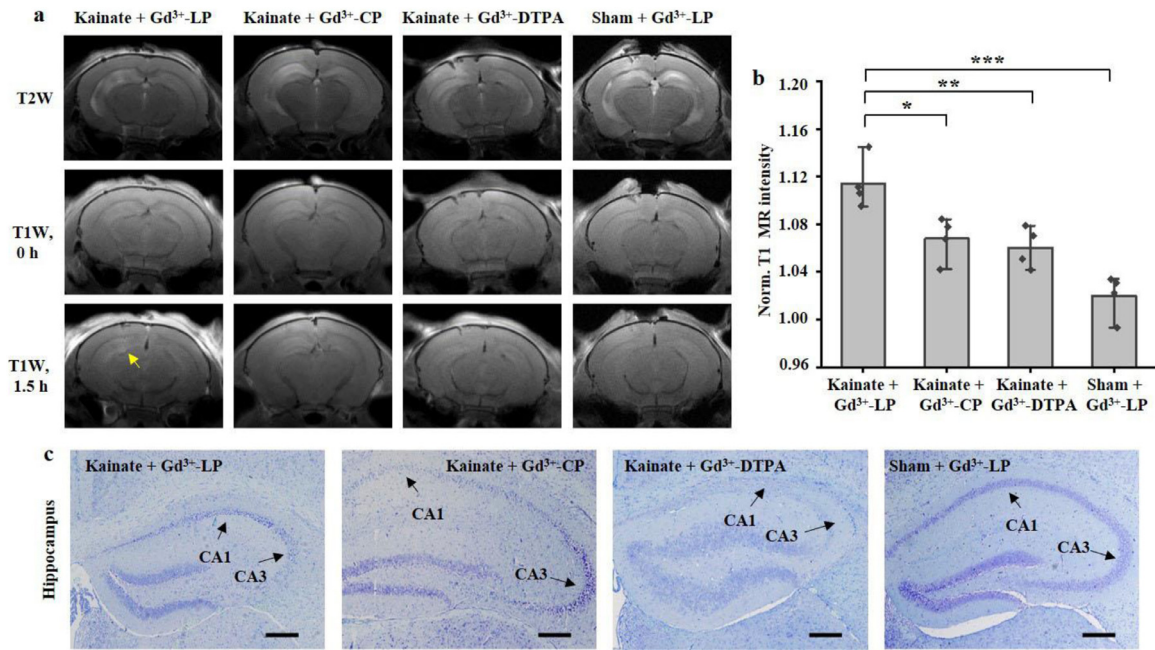
Fig. 6. Gd^{3+}-LP defining the epileptic foci in kainate models. (a) Representative coronal T1-weighted MR images of the chronic epileptic mouse or sham mouse brain at 1.5 h post the administration of Gd^{3+}-LP or Gd^{3+}-CP with the same Gd^{3+} concentration (0.1 mmol/kg). The epileptic foci with hyperintensive T1W MR signal induced by Gd^{3+}-LP was pointed out by yellow arrow. (b) Normalized T1-weighted MR signal intensities in the epileptic foci after the above treatments. (n = 4), unpaired two-tailed Student's t tests. (c) White-light microscopic images of mouse brain sections after Nissl staining. Arrows point to the injured neurons or normal neurons in the ipsilateral hippocampus CA1 and CA3 subfields. Upper row (Scale bar = 200 μm); Middle and bottom rows (Scale bar = 50 μm). Norm. = normalized. $^*P < 0.05$. $^{***}P < 0.01$, $^{***}P < 0.001$, unpaired two-tailed Student's t-tests.

Simultaneously, clear paroxysmal discharges were observed. In the latent period, no obvious abnormal behaviours and occasionally interictal spikes were recorded. More than 80% of kainate-treated mice were developed as chronic models with spontaneous seizures and spontaneous paroxysmal discharge after 8–20 days post status epilepticus. Neuroinflammatory events involving glial function dysregulation are evident in the different phases of epileptogenesis and may be regarded as a prominent feature of epileptic foci [14]. The immunofluorescence results showed that astrocytes in the mouse hippocampus kept activated and eventually formed glial scars in chronic epilepsy models. The extent of microglial activation in the acute and chronic phases was more obvious than that in the latent phase. The resurgence of activated microglia was found in the chronic phase, which is potentially related to spontaneous seizures and may contribute to further seizure generation by releasing proinflammatory molecules [32]. Notably, the expression level of LRP1 correlated with the extent of glial activation and the LRP1 level increased substantially in the acute and chronic phases.

SPECT imaging has superiority in sensitivity and quantifiability, which provides the convenience to investigate the sensitivity of the probe and the expression level of LRP1 in the epileptic lesions. Considering that the DTPA chelators in the Gd^{3+}-LP could conjugate both Gd^{3+} and ^{99m}Tc, we developed a radioactive derivative ^{99m}Tc-LP with a similar structure with Gd^{3+}-LP. Higher ^{99m}Tc-LP uptake in the ipsilateral hemisphere than the contralateral hemisphere indicated the up-regulation of LRP1 during epileptogenesis. Furthermore, the higher ipsilateral to contralateral hemisphere uptake ratio of ^{99m}Tc-LP than ^{99m}Tc-CP verified the LRP1-targeting specificity.

Based on the SPECT imaging results, we further tested if the LRP1-targeted strategy could image the epileptic foci with MR, which is essential for presurgical assessment of epileptic foci due to its excellent spatial resolution to soft tissues. The chronic model with spontaneous seizures is a better choice to mimic temporal lobe epilepsy patients and was selected for in vivo MRI studies. Hyperintense T2 signals in the ipsilateral hippocampus were observed in chronic seizure mice, which can be attributed to the reactive gliosis or edema

confirmed by immunofluorescence staining [33]. Noticeable T1-weighted MR signal enhancement with Gd^{3+}-LP was observed in the ipsilateral hippocampus where kainate was injected. The lesion location accuracy was verified by interictal ^{18}F-FDG PET, in which the hypometabolism cerebral area was consistent with the high T1W MR signal area. *Ex vivo* Nissl staining also verified the accuracy of Gd^{3+}-LP in defining the epileptic region. Noticeable, no obvious T1W-MR signal enhancement was observed in chronic kainate models after intravenous administration of paramagnetic contrast agents Gd^{3+}-DTPA, which implies the BBB integrity of kainate models could be substantially restored during the chronic phase. Although van Vliet et al. found minor BBB leakage in kainate rats using step-down infusion of gadobutrol in combination with T1-weighted MRI (post−pre approach) and fast T1 mapping (dynamic approach), these MRI approaches are hardly implemented in routine clinical settings due to complicated dynamic scanning protocols [34]. Additionally, because of the good reproducibility and high similarity to human temporal lobe epilepsy, kainate models in chronic phase were widely used in studies for locating the epileptogenic region [31].

In the past decade, the excitatory neurotransmitter receptors (e.g. N-methyl-D-asparate glutamate receptor and γ-aminobutyric acid receptor), multidrug transporter receptors (e.g. P-glycoprotein), and inflammation receptor (e.g. TSPO and VCAM-1) have been screened to define the MRI negative epilepsy foci [9,35,36]. Compared to the above biomarkers, LRP1 demonstrates numerous advantages. First, the LRP1-mediated BBB traverse and its upregulation in multiple cell types may benefit the visualisation of the epileptic foci with higher sensitivity than the receptors expressed exclusively on neurons or glia. Second, the LRP1-targeted radiotracer holds the promise to delineate the "concealed" epileptic region by crossing the intact BBB. Third, improved imaging specificity can be achieved with LRP1-targeted radiotracer through a two-order targeted strategy. In this strategy, the probe first targets the LRP1 overexpressed luminal face of the inflammatory vasculatures, followed by endothelial traverse via receptor-mediated transcytosis. After penetrating the BBB, the probe targets the LRP1 overexpressed activated microglia and astrocytes in

the epileptic foci. Due to the bidirectional BBB transport property of LRP1 [16], the non-specifically distributed probes in the normal brain tissue could be timely excreted from the brain to the blood, which improves the imaging specificity.

Several limitations still existed in the present study. First, multiple causes can induce epilepsy, which in general include structural abnormality, genetic mutation, infectious risk, metabolic disturbance and other unknown aetiologies [37]. However, only one type of seizure model was used in this study. The temporal and spatial distribution of LRP1 expression in other types of epileptic models needs further investigations. Second, although the temporal and spatial expression of LRP1 during epileptogenesis in the kainate models was studied, the exact mechanism of the neuroinflammation triggered LRP1 up-regulation needs to be clarified in future. Last but not least, BBB leakage was evident during the acute phase after kainite injection. Even though the BBB integrity of kainate models could be restored to a large extent during the chronic phase, subtle BBB leakage is indeed present in the lesions. The effectiveness of the LRP1-targeted probe in delineating the epileptic foci needs to be tested in other epilepsy models with relatively intact BBB structure.

In conclusion, we demonstrated that the BBB remained partially intact in the epileptic foci of DRE patients. The up-regulation of an inflammation-associated biomarker LRP1 in the epileptic regions of both DRE patients and epileptic models was verified. Then an LRP1-targeted probe was developed, which can visualise the epileptic foci in kainate models with the improved target to background ratios. Overall, this LRP1-targeted imaging strategy is promising and can be a complement to the existing diagnostic technologies used to locate the "concealed" epileptic foci in DRE patients.

Contributors

All authors reviewed the report and approved the final version. Guarantors of integrity of entire study, Cong Wang, Jianping Zhang, Shaoli Song, Ying Mao, Hao Wang, Liang Chen, Cong Li; study concepts/study design or data acquisition or data analysis/interpretation, all authors; manuscript drafting or manuscript revision for important intellectual content, all authors; approval of the final version of the submitted manuscript, all authors; agrees to ensure any questions related to the work are appropriately resolved, all authors; literature research, Cong Wang, Zhi Li, Shujie Yin, Zixuan Wei, Ying Mao, Hao Wang, Liang Chen, Cong Li; experimental studies, Cong Wang, Jianping Zhang, Zhi Li, Shujie Yin, Wenjia Duan, Zixuan Wei, Ming Qi, Wanbing Sun, Lu Zhang, Luo Chen, Xihui Gao; statistical analysis, Cong Wang, Jianping Zhang, Shaoli Song, Xihui Gao, Wanbing Sun, Lu Zhang; guarantors of the accuracy of the raw data, Cong Wang, Jianping Zhang, Zhi Li, Shujie Yin, Wenjia Duan, Ming Qi, Lu Zhang; and manuscript editing, Cong Wang, Shaoli Song, Zhi Li, Shujie Yin, Wenjia Duan, Wanbing Sun, Ying Mao, Hao Wang, Liang Chen, Cong Li.

Declaration of Competing Interest

The authors declare that they have no conflicts of interest.

Acknowledgements

Data sharing statement

The main data supporting the findings of this study are available within the paper and its Supplementary Information. All data generated, both raw images and analysed datasets, for the figures in this study were uploaded with the manuscript and can be download at 10.17632/fwwhp72pzy.1 (https://data.mendeley.com/).

Supplementary materials

Supplementary material associated with this article can be found, in the online version, at doi:10.1016/j.ebiom.2020.103156.

References

[1] Thurman DJ, Beghi E, Begley CE, et al. Standards for epidemiologic studies and surveillance of epilepsy. Epilepsia 2011;52:2–26.
[2] Kwan P, Schachter SC, Brodie MJ. Drug-resistant epilepsy. New Engl J Med 2011;365(10):919–26.
[3] Wiebe S, Jetté N. Epilepsy surgery utilization: who, when, where, and why? Curr Opin Neurol 2012;25(2):187–93.
[4] Olson LD, Perry MS. Localisation of epileptic foci using multimodality neuroimaging. Int J Neural Syst 2013;23(01):1230001.
[5] Téllez-Zenteno JF, Ronquillo LH, Moien-Afshari F, Wiebe S. Surgical outcomes in lesional and non-lesional epilepsy: a systematic review and meta-analysis. Epilepsy Res 2010;89(2-3):310–8.
[6] Duncan JS, Winston GP, Koepp MJ, Ourselin S. Brain imaging in the assessment for epilepsy surgery. Lancet Neurol 2016;15(4):420–33.
[7] Davis KA, Nanga RPR, Das S, et al. Glutamate imaging (GluCEST) lateralizes epileptic foci in nonlesional temporal lobe epilepsy. Sci Transl Med 2015;7 (309):309ra161.
[8] Walker LE, Janigro D, Heinemann U, Riikonen R, Bernard C, Patel M. WONOEP appraisal: molecular and cellular biomarkers for epilepsy. Epilepsia 2016;57 (9):1354–62.
[9] Pitkanen A, Loscher W, Vezzani A, et al. Advances in the development of biomarkers for epilepsy. Lancet Neurol 2016;15(8):843–56.
[10] Bien CG, Szinay M, Wagner J, Clusmann H, Becker AJ, Urbach H. Characteristics and surgical outcomes of patients with refractory magnetic resonance imaging-negative epilepsies. Arch Neurol-Chicago 2009;66(12):1491–9.
[11] Duncan JS. Imaging in the surgical treatment of epilepsy. Nat Rev Neurol 2010;6 (10):537–50.
[12] Cohen-Gadol AA, Wilhelmi BG, Collignon F, et al. Long-term outcome of epilepsy surgery among 399 patients with nonlesional seizure foci including mesial temporal lobe sclerosis. J Neurosurg 2006;104(4):513–24.
[13] Vezzani A, French J, Bartfai T, Baram TZ. The role of inflammation in epilepsy. Nat Rev Neurol 2011;7(1):31–40.
[14] Devinsky O, Vezzani A, Najjar S, De Lanerolle NC, Rogawski MA. Glia and epilepsy: excitability and inflammation. Trends Neurosci 2013;36(3):174–84.
[15] Gonias SL, Campana WM. LDL receptor-related protein-1: a regulator of inflammation in atherosclerosis, cancer, and injury to the nervous system. Am J Pathol 2014;184(1):18–27.
[16] Gao X, Yue Q, Liu Z, et al. Guiding brain−tumor surgery via blood-brain−barrier−permeable gold nanoprobes with acid−triggered MRI/SERRS signals. Adv Mater 2017;29(21):1603917.
[17] Guo Q, Zhu Q, Miao T, et al. LRP1-upregulated nanoparticles for efficiently conquering the blood-brain barrier and targetedly suppressing multifocal and infiltrative brain metastases. J Control Release 2019;303:117–29.
[18] Jo I, Im HM, Shin HJ, et al. Serum deprivation increases the expression of low density lipoprotein receptor-related protein in primary cultured rat astrocytes. Biochem Bioph Res Co 2002;299(1):102–8.
[19] Hendrickx DA, Koning N, Schuurman KG, et al. Selective upregulation of scavenger receptors in and around demyelinating areas in multiple sclerosis. J Neuropathol Exp Neurol 2013;72(2):106–18.
[20] Kim KS, Park W, Hu J, Bae YH, Na K. A cancer-recognizable MRI contrast agents using pH-responsive polymeric micelle. Biomaterials 2014;35(1):337–43.
[21] Racine RJ. Modification of seizure activity by electrical stimulation: II. Motor seizure. Electroen Clin Neuro 1972;32(3):281–94.
[22] Maroso M, Balosso S, Ravizza T, et al. Toll-like receptor 4 and high-mobility group box-1 are involved in ictogenesis and can be targeted to reduce seizures. Nat Med 2010;16(4):413.
[23] Balosso S, Maroso M, Sanchez-Alavez M, et al. A novel non-transcriptional pathway mediates the proconvulsive effects of interleukin-1β. Brain 2008;131 (12):3256–65.
[24] La Fougère C, Rominger A, Förster S, Geisler J, Bartenstein P. PET and SPECT in epilepsy: a critical review. Epilepsy Behav 2009;15(1):50–5.

[25] Tang W, Fan WP, Lau J, Deng LM, Shen ZY, Chen XY. Emerging blood-brain-barrier-crossing nanotechnology for brain cancer theranostics. Chem Soc Rev 2019;48(11):2967–3014.

[26] Huber JD, Egleton RD, Davis TP. Molecular physiology and pathophysiology of tight junctions in the blood-brain barrier. Trends Neurosci 2001;24(12):719–25.

[27] Patel MM, Patel BM. Crossing the blood-brain barrier: recent advances in drug delivery to the brain. Cns Drugs 2017;31(2):109–33.

[28] Wang X, Liu GH, Chen N, et al. Angiopep2-conjugated star-shaped polyprodrug amphiphiles for simultaneous glioma-targeting therapy and MR imaging. ACS Appl Mater Inter 2020;12(10):12143–54.

[29] Wahsner J, Gale EM, Rodriguez-Rodríguez A, Caravan P. Chemistry of MRI contrast agents: current challenges and new frontiers. Chem Rev 2018;119(2):957–1057.

[30] Gao XH, Qian J, Zheng SY, et al. Up-regulating blood brain barrier permeability of nanoparticles via multivalent effect. Pharm Res-Dordr 2013;30(10):2538–48.

[31] Lévesque M, Avoli M. The kainic acid model of temporal lobe epilepsy. Neurosci Biobehav R 2013;37(10):2887–99.

[32] Benson MJ, Manzanero S, Borges K. Complex alterations in microglial M1/M2 markers during the development of epilepsy in two mouse models. Epilepsia 2015;56(6):895–905.

[33] Von Oertzen J, Urbach H, Blumcke I, et al. Time-efficient T2 relaxometry of the entire hippocampus is feasible in temporal lobe epilepsy. Neurology 2002;58(2):257.

[34] van Vliet EA, Otte WM, Gorter JA, Dijkhuizen RM, Wadman WJ. Longitudinal assessment of blood-brain barrier leakage during epileptogenesis in rats. A quantitative MRI study. Neurobiol Dis 2014;63:74–84.

[35] Duffy BA, Choy MK, Riegler J, et al. Imaging seizure-induced inflammation using an antibody targeted iron oxide contrast agent. Neuroimage 2012;60(2):1149–55.

[36] Brackhan M, Bascunana P, Postema JM, et al. Serial quantitative TSPO-targeted pet reveals peak microglial activation up to 2 weeks after an epileptogenic brain insult. J Nucl Med 2016;57(8):1302–8.

[37] Moshé SL, Perucca E, Ryvlin P, Tomson T. Epilepsy: new advances. Lancet 2015;385(9971):884–98.